

Chapter 1

Jet Gravitational Waves

Tsvi Piran

*Racah Institute for Physics,
The Hebrew University, Jerusalem, 91904, Israel,
tsvi.piran@mail.huji.ac.il*

The acceleration of a jet to relativistic velocities produces a unique memory type gravitational waves (GW) signal: *Jet-GW*. I discuss here recent results concerning properties of these GWs and consider their detectability in current and proposed detectors. Classical sources are long and short Gamma-ray bursts as well as hidden jets in core-collapse supernovae. Detection of jet-GWs from these sources will require detectors, such as the proposed BBO, DECIGO and lunar based detectors, that will operate in the deciHz band. The current LIGO detectors could detect jet-GWs from a Galactic SGR flare if it is sufficiently asymmetric. Once detected these signals could reveal information concerning jet acceleration and collimation that cannot be explored otherwise.

1. Introduction

The detection of gravitational waves from merging compact objects (black holes and neutron stars) binaries opened a new era in Physics and Astronomy.^{1,2} The current detectors have been upgraded and new detectors at other wavelengths are being planned. On the theory side new prospects for detection and utilization of gravitational waves from different sources have been proposed. One such less explored source - *gravitational waves from relativistic jets: Jet-GWs*.

Any relativistic jet involves acceleration of mass (or energy density - if the jet is Poynting flux dominated) from rest to a speed approaching the speed of light. This acceleration process produces a memory type gravitational waves signal³⁻⁷ (see Fig. 1). A low frequency detector, will “see” this signal as a sudden jump. A higher frequency whose frequency range is comparable to the rise time of this signal, will resolve a temporal structure that can reveal the nature of the jets and the acceleration process. In this article I review the basic features of *Jet-GWs* and discuss potential sources and detection prospects.

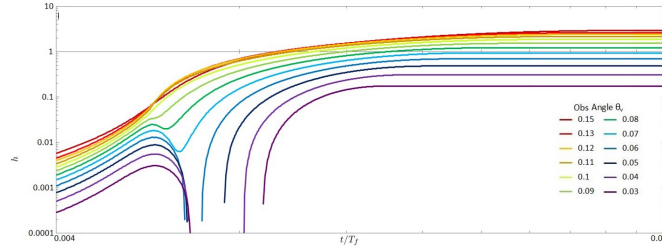


Fig. 1. The normalized GW amplitude, $h(t)$, for a jet with an opening angle $\theta_j = 0.1$ and a final Lorentz factor, $\Gamma = 100$ for different observer angles. From ref. [6].

2. Instantaneously accelerate point particle

Consider, first, a point mass m that is instantaneously accelerated to a Lorentz factor Γ . The total energy is $\mathcal{E} = m\Gamma$ (unless specified otherwise I use units in which $c=G=1$). While non-physical, this limit gives an excellent idea of the emerging patterns. The waveform is a Heaviside step function:

$$h(t, \theta_v) = h(\theta_v) \mathcal{H}(t), \quad (1)$$

where θ_v is the angle between the direction of the motion of the particle and the line of sight to the distant observer in the observer's frame of reference (see Fig. 2).

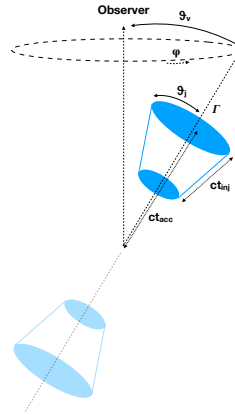


Fig. 2. A schematic description of the jet. The top shell has reached the final Lorentz factor at a distance ct_{acc} from the origin. The duration of mass injection is t_{inj} . A counter-jet is shown in light colors. From ref.[7].

The Fourier transform is given by

$$\tilde{h}(f, \theta_v) = h(\theta_v)/f. \quad (2)$$

The gravitational wave amplitudes h_+ and h_x of the two polarization modes are given by:³

$$h^{TT}(\theta_v) = h_+ + ih_x = \frac{2\mathcal{E}\beta^2}{r} \frac{\sin^2 \theta_v}{1 - \beta \cos \theta_v} e^{2i\phi}, \quad (3)$$

where ϕ is an azimuthal angle. For a single point-particle, the phase, $2i\phi$, can be ignored. When discussing the metric perturbation of an ensemble of particles the complex phase leads to an interference and must be taken into account.

The angular dependence of $h(\theta_v)$ is shown in Fig. 3. It exhibits anti-beaming: the GW amplitude vanishes along its direction of motion. It remains small at a cone around it, reaching 50% of the maximal values at an opening angle Γ^{-1} . The function $h(\theta_v)$ attains a maximum of

$$h_{\max} = \frac{4G\mathcal{E}}{c^4 r} \frac{\Gamma}{\Gamma + 1}, \quad \text{at } \theta_{\max} = \cos^{-1}\left[\frac{1 + \Gamma}{\beta\Gamma}\right] \approx \sqrt{\frac{2}{\Gamma}}, \quad (4)$$

where r is the distance to the source and for clarity Newton's constant, G , and the speed of light, c , have been added to this equation. Interestingly, this relation resembles the classical quadrupole relation for the GW amplitude $h_{\max} \propto (GM/c^2 r)(v/c)^2$ (with $v = c$), even though the quadrupole approximation is not valid in this case.

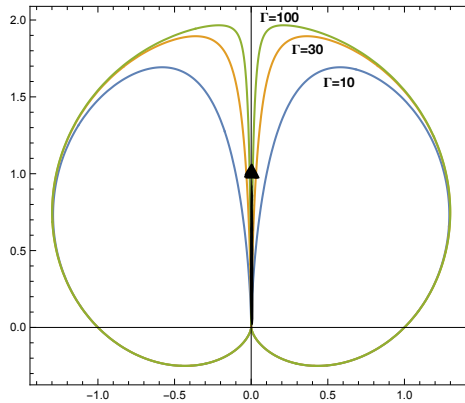


Fig. 3. An antenna pattern for the GW amplitude, h , from an instantaneously accelerated point-like jet for different Lorentz factors. h is anti-beamed with an opening angle Γ^{-1} around the jet direction.

The GW energy is beamed in the forward direction (see Fig. 3). 50% of the GW energy is deposited in a cone with an opening angle $\theta_{50\%} = \sqrt{2/\Gamma}$.

In many cases there are two jets moving in opposite directions. The GW amplitude in this case is the sum of the two signals:

$$h(\theta_v) = \frac{4\mathcal{E}\beta^2}{r} \frac{1 - \cos^2 \theta_v}{1 - \beta^2 \cos^2 \theta_v}, \quad (5)$$

(see Fig. 4). This signal is almost flat apart from two narrow *anti-beams* of width Γ^{-1} along the directions of the jets. The energy is, however, still beamed into two regions of width $\sqrt{2/\Gamma}$ along the jets. Note, that these figures, that depicts $h(\theta_v)$ are somewhat misleading. While they depict the correct value of h they

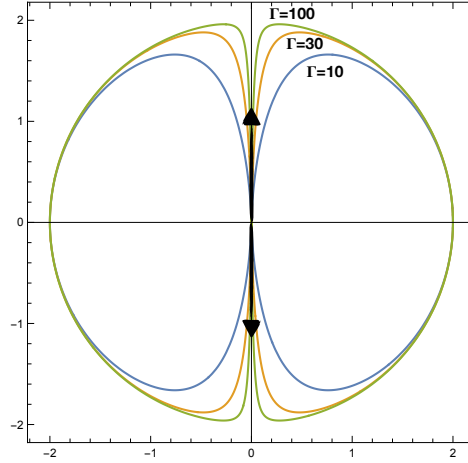


Fig. 4. An antenna pattern for the GW amplitude, h , from two opposite jets for different Lorentz factors. h is almost uniform, apart from being anti-beamed with an opening angle Γ^{-1} around the jets directions.

ignore a critical factor - the characteristic time scale. This time scale that strongly influences the detectability (as well as the energy flux) may varies with θ_v .

Recalling Eq. 2 we note that formally the total GW energy emitted,

$$E_{\text{GW}} = \frac{1}{32\pi} \iint \left(\frac{\partial h}{\partial t} \right)^2 dt d\Omega = \frac{1}{32\pi} \iint \tilde{h}(f)^2 f^2 df d\Omega, \quad (6)$$

diverges for an instantaneously accelerating particle. This divergence is not physical as it arises from the instantaneous approximation. If the system has a typical timescale t_c than there should be an upper cutoff to the frequency above which $h(f)$ decreases with f much faster than f^{-1} and the integral is finite.

The overall energy emitted is of order:⁷

$$E_{\text{GW}} = F(\Gamma) [G\mathcal{E}/c^5 t_c] \mathcal{E}, \quad (7)$$

where $F(\Gamma)$ is a function of the jet's final Lorentz boost. $F(\Gamma)$ vanishes when $\beta \rightarrow 0$. When $\Gamma \rightarrow \infty$ the situation is more complicated and in extreme cases we have to take into account the details of the acceleration process to properly estimate the energy emitted. Note that the factor in square brackets is always smaller than unity.

3. Time Scales and the Temporal Structure

The above considerations stress the importance of the characteristic time scale. There are two timescales in the system and the relevant one is of course the longest. The two intrinsic time scales are the injection timescale, t_{inj} that is measured in the observer's rest frame (which is the same as the source rest frame). It characterizes the overall duration of the jet. A second intrinsic time scale, t_{acc} , characterizes the acceleration (it is also measured in the source rest frame).

The signal is determined by t_{acc} via the arrival time from different angular regions of the jet. The arrival time is related to t_{acc} as:

$$t_o(\theta_v) = (1 - \beta \cos \Delta\theta_v)t_{\text{acc}}, \quad (8)$$

where β is the jet's velocity and $\Delta\theta_v = \theta_v + \theta_j$ is the sum of θ_v and the angular width of the jet, θ_j (see fig:geometry). t_o is the time difference from the observation of the beginning of the acceleration and the arrival time of the signal from the furthest point of the jet from observer (see Fig. 2).

The observed time scale of the GW signal, t_c , is the longest between t_{inj} and t_o :

$$t_c(\theta_v) = \max(t_{\text{inj}}, t_o) = \max[t_{\text{inj}}, (1 - \beta \cos \Delta\theta_v)t_{\text{acc}}]. \quad (9)$$

As t_o depends on the viewing angle, the dominant time scale may be t_{inj} for some observers and t_o for others. More specifically, t_{inj} is independent of the viewing angle. On the other hand $t_o \ll t_{\text{acc}}$ for small viewing angles. Thus unless t_{acc} is very large, $t_c = t_{\text{inj}}$ for these angles. However t_o becomes significantly larger when $\Delta\theta$ increases and for those angles we may have $t_c = t_o$.

The Fourier transform of a memory-type signal that is rising to an asymptotic value $h_0(\theta_v)$ over a timescale t_c , has a general shape:

$$\tilde{h}(f, \theta_v) = \begin{cases} h_0(\theta_v)/f, & f \leq f_c \\ h_0(\theta_v)g(f/f_c)/f_c, & f \geq f_c. \end{cases} \quad (10)$$

The crossover frequency, f_c , in which the Fourier transform of the GW signal changes its behavior is the reciprocal of the time scale, t_c : $f_c \equiv 1/t_c$. The function $g(f/f_c)$ depends on the nature of the source. It always decreases faster than $(f/f_c)^{-1}$. As the total GW energy must be finite, the integral $\int_0^\infty \dot{h}^2(t)dt = \int_0^\infty f^2 \tilde{h}^2(f)df$ yields an asymptotic bound of $g \propto (f/f_c)^{-\alpha_{\text{inf}}}$ with $\alpha_{\text{inf}} > 3/2$.

The spectral density, $S(f) \equiv \tilde{h}(f) \cdot \sqrt{f}$, is used to characterize the sensitivity of GW detectors.

$$S(f, \theta_v) = \begin{cases} h_0(\theta_v)/f^{1/2}, & f \leq f_c \\ h_0(\theta_v)g(f/f_c)f^{1/2}/f_c, & f \geq f_c. \end{cases} \quad (11)$$

The spectral density at the crossover frequency, $S(f_c) = h_0(\theta_v)/f_c^{1/2}$, is critical to determine the detectability of the signal. The condition

$$S_{\text{det}}(f) < S(f_c)(f_c/f)^{1/2} = h_0(\theta_v)/f^{1/2} \quad \text{for some } f, \quad (12)$$

is a necessary condition for detection. For a low-frequency detector (whose typical frequency range is below f_c) this condition is sufficient. However, it is not sufficient for a high frequency detector as $S(f)$ decreases faster than $f^{-1/2}$ above f_c .

A more detailed discussion of the Fourier transform, $\tilde{h}(f, \theta_v)$ and the spectral density is given in ref. [7]. As an example Fig. 5 depicts \tilde{h} for different jets.

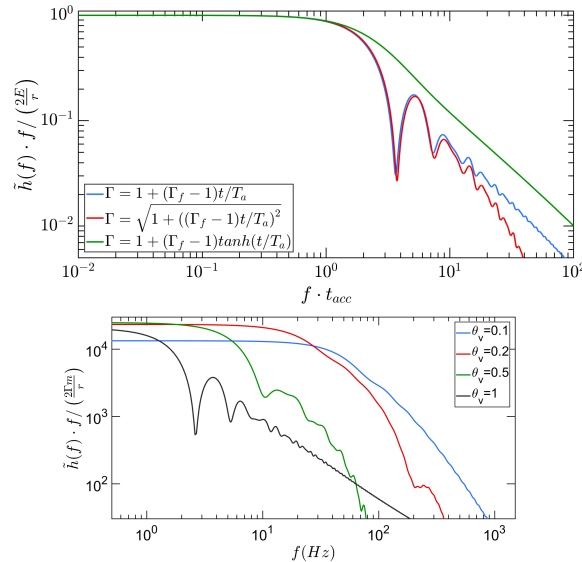


Fig. 5. *top*: The Fourier transforms, \tilde{h} of the GW signals from jets with three different acceleration models (with $\Gamma_f = 100$, $\theta_j = 0.1$, $\theta_v = 0.9$). In all cases $t_{\text{inj}} = 0$. The time constant of the third model was chosen such that the high-frequency power laws would coincide. *Bottom*: The normalized Fourier waveform multiplied by the frequency for jets with the acceleration model $\Gamma \propto R$, based on the numerical code describe in⁶ for $\Gamma = 100$ and $\theta_j = 0.1$. Below the crossover frequency, $\tilde{h}(f) \cdot f$ is a constant. From ref.[7].

4. The Angular Structure

To explore the effect of the angular width of the jet we consider a thin spherical shell ejected simultaneously and accelerated instantaneously. The shell has a half opening angle θ_j and its center is moving at an angle θ_v relative to the observer. If $\theta_j \lesssim \Gamma^{-1}$ the signal converges to the point-particle limit. So in the rest we consider the case of $\Gamma^{-1} \ll \theta_j$. Otherwise cancellations between different parts of the shell become significant and the signal becomes weaker with a broader anti-beaming region around the axis.

We define the observer's line of sight to the emitting source as the z axis of our coordinate system. The coordinates θ and ϕ are defined in the observer's coordinate system in the usual manner (see Fig. 2). The direction of the center of the jet is $(\theta, \phi) = (\theta_v, 0)$ in the observer's frame of reference. The axial symmetry implies a symmetry under the transformation $\phi \rightarrow -\phi$. Therefore, the metric perturbation h_x (which is now summed over the shell) vanishes identically (see Eq. 3, and Fig. 6). In the following, we simply denote $h = h_+$, the only non-vanishing component of the metric perturbation tensor.

Integrating over the shell we find:

$$h(\theta_v, \theta_j) = \frac{2\mathcal{E}\beta^2}{r\Delta\Omega} \int_{|\theta_v - \theta_j|}^{\min(\theta_j + \theta_v, \pi)} \frac{\sin^3 \theta \cdot \sin 2\Delta\phi}{1 - \beta \cos \theta} d\theta, \quad (13)$$

where $\Delta\Omega \equiv 2\pi(1 - \cos\theta_j)$, the solid angle of the cap, and

$$\Delta\phi \equiv \cos^{-1} \left[\frac{\cos\theta_j - \cos\theta_v \cos\theta}{\sin\theta_v \sin\theta} \right]. \quad (14)$$

Figure 7 depicts the antenna pattern of $h(\theta_v, \theta_j)$ for different opening angles. This angular behavior resembles the point-particle result, with a major difference:

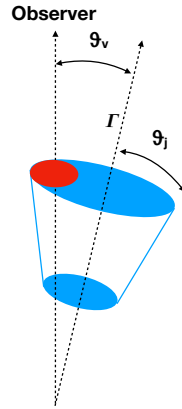


Fig. 6. A schematic view of the jet (blue) for $\theta_v < \theta_j$. Due to the symmetry, the contribution to the GW amplitude of the part of the jet that is spherically symmetric around the observer (shown in red) vanishes. The amplitude from partial rings with $\theta > \theta_j - \theta_v$, is reduced compared to the amplitude of a point-particle with the same energy and angle to the observer. The jet is symmetric under the transformation $\phi \rightarrow -\phi$: hence, the metric perturbation component h_x vanishes identically. From ref.[7].

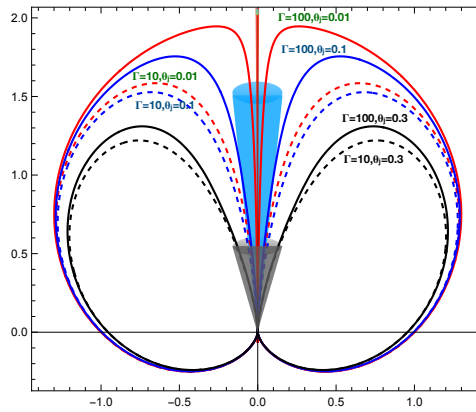


Fig. 7. Antenna pattern for the GW amplitude, h , from an accelerating spherical shells with different opening angles ($\theta_j = 0.01, 0.1, 0.3$ - red, blue and black) and different Lorentz factors ($\Gamma = 10, 100$ - dashed and solid lines). The anti-beaming region is $\approx 0.84 \theta_j$. The narrow jet with $\theta_j = 0.01 \approx \Gamma^{-1}$ behaves like a point particle. For the larger opening angles ($\theta_j > \Gamma^{-1}$) the pattern is almost independent of Γ .

the anti-beaming region, which was Γ^{-1} in the point-particle case, is now $\approx 0.84 \theta_j$ and it is independent of Γ (if $\Gamma^{-1} < \theta_j$). If the jet is wide the signal is also weaker because of the cancellation of the signals from different parts of the shell. For $\theta_v < \theta_j$, only the outer region of the shell, with $\theta > \theta_j - \theta_v$, contributes. The effect is twofold: regions of the shell with $\theta < \theta_j - \theta_v$ have a vanishing contribution to the amplitude, and even in the outer region, destructive interference between symmetric regions will reduce the GW amplitude. The maximal GW amplitude is now a function of θ_j (compare with Eq. 4). For small opening angles:

$$h_{\max}(\theta_j) \approx \frac{4\mathcal{E}}{r} \left(1 - \frac{3}{4}\theta_j\right). \quad (15)$$

Like in the case of a point source the GW signal of two sided jets with angular structure will be the sum of the two signals of the form given by Eq. 13. The amplitude of h will be almost isotropic but now with wider anti-beamed regions along the jets directions. Again the energy flux will be predominantly in the forward directions of the two jets.

5. Detectability

To estimate detectability, we compare the expected spectral density, $S(f)$, to the detector's sensitivity curve that is characterized by $S_{\text{det}}(f)$. $S(f)$ is always a decreasing function of the frequency. At low frequencies, namely for $f < f_c$, $S(f) \propto f^{-1/2}$. It decreases faster for $f > f_c$. A typical low-frequency detector will be most sensitive to a jet-GW signal at the lowest end of its frequency response. Namely, the lowest frequency below which S_{det} is steeper than $f^{-1/2}$. At high-frequencies ($f > f_c$) $S \propto f^{-\alpha}$ with $\alpha > 1/2$. A high-frequency detector is most sensitive for this signal at its lowest frequency below which S_{det} is steeper than $f^{-\alpha}$.

Like almost any GW source involving a relativistic motion, the maximal amplitude of the jet GW is of order

$$h \approx \frac{4G\mathcal{E}}{c^4 r} \approx 10^{-24} \left(\frac{\mathcal{E}}{10^{51} \text{ erg}} \right) \left(\frac{100 \text{ Mpc}}{r} \right). \quad (16)$$

$h = 10^{-24}$ is lower than the sensitivity of current GW detectors. Additionally, as we discuss later, these detectors don't operate in the deciHz frequency range that is relevant for most sources. However, we have to remember that the sensitivity of current and planned detectors is much nearer to this signal than the situation at the early 90ies when efforts to construct LIGO and Virgo begun.

For a one-sided jet this estimate is valid for an observer that is at optimal angle, namely at $\theta_v \approx \theta_j$. For two-sided jets, this estimate is valid for most observers apart from those along the jets ($\theta_v < \theta_j$). Different observers may observe different characteristic crossover frequencies (see Eq. 9). In the following we will focus on observers that are in the forward direction (but not within the anti-beaming cones).

6. Potential Sources

Detection horizons can be obtained by comparing the crossover frequency and amplitude of potential sources with the characteristics frequencies and noise amplitudes of several detectors. Given the uncertainties in the signals and in properties of planned detectors this simple approach is sufficient at this stage. Table 1. summarizes the basic features of the different sources and their detection horizon (assuming the high end of the energy range, a viewing angle near the jet and the most suitable frequency) with different GW detectors.

Table 1. Horizon distances of several current and proposed detectors for different sources. Fig. 8 describes the sensitivity curves of LVK, Einstein telescope, BBO and DECIGO. For a moon type detector such as LWGA¹⁰ or LSGA¹¹ I use sensitivity of $10^{-22}/\sqrt{Hz}$ at $10^{-3}Hz$. The values are given using optimistic values of the energy (maximal) and the viewing angle (just outside the anti-beaming cone).

Source	Energy \mathcal{E} (erg)	Frequency f_c (Hz)	Typical Distance	LVK	Einstein Telescope	BBO	DECIGO	Moon ^{10,11} detectors
LGRB	10^{50-52}	0.1-0.01	6 Gpc	-	-	Gpc	500 Mpc	30 Mpc
sGRB	10^{48-50}	1-10	1 Gpc	-	5 Mpc	75 Mpc	50 Mpc	3 Mpc
Sn Jet	10^{50-51}	0.1-0.01	100 Mpc	-	-	100 Mpc	50 Mpc	3 Mpc
SGR	10^{46-47}	0.001	10 kpc	2.5 kpc	25 kpc	750 kpc	500 kpc	10 kpc

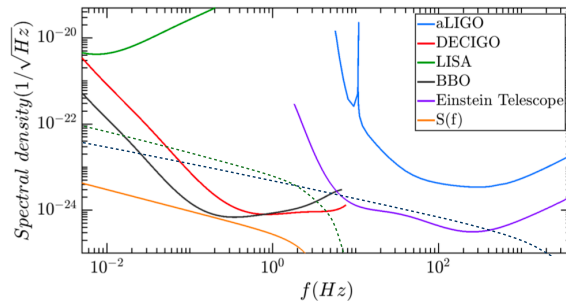


Fig. 8. The estimated spectral density for a fiducial model⁷ of GW170817, $S(f)$, compared with the sensitivity thresholds of GW detectors taken from <http://gwplotter.com>.⁸ The dotted red line shows the GW emission from a CCSN jet with 10^{51} erg at 20 Mpc. The dotted black line corresponds to a Galactic SGR flare of 10^{47} erg at 10kpc. Adapted with modifications from ref. [7].

6.1. GRBs

GRB jets that have motivated these ideas^{3,4} seems to be the most natural sources for these kind of GWs. These powerful ultra-relativistic jets carry up to 10^{52} erg (for long GRBs) and 10^{50} erg (for short ones). Given the numerous other differences between the two populations (long GRBs are typically detected from larger distances

and they have significantly larger t_{inj}) we consider each subgroup independently. The crossover frequency is dominated by t_{inj} for both long and short GRBs. Thus, $f_c = f_l = 0.1 - 0.01$ Hz for the long and $f_c = f_s = 1 - 10$ Hz for short GRBs. This frequency range puts the events below the frequency limits of current LIGO-Virgo-Kagra, but around the capability of the planned Big Bang Observer (BBO)¹² and DECIGO.¹³

6.1.1. Long GRBs

Long GRBs (LGRBs) are associated with Collapsars - collapsing massive stars. Their typical isotropic equivalent energies range from 10^{51-54} ergs. When taking into account beaming, which is typically of order $\theta_j \approx 0.1 - 0.2$ rad (but highly uncertain) this corresponds to $\mathcal{E} \approx 10^{50-52}$ erg. With typical distances of a few Gpc the GW amplitude from a regular LGRBs is quite low $\sim 10^{-26}$. The duration of LGRBs ranges from 2 sec to a few hundred seconds, with typical duration of ~ 20 sec.

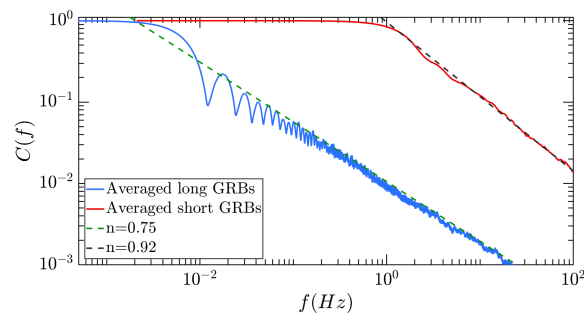


Fig. 9. The averaged Fourier transform of BATSE's long GRBs,¹⁴ vs. that of BATSE's TTE short GRB catalogue.⁷ Power law fits for are shown in dashed lines. From ref. [7].

The average power spectrum of the bursts' γ -rays light curve shows a crossover frequency of $\approx 10^{-2}$ Hz.¹⁴ This crossover frequency reflects the overall duration of the bursts. If the duration of the γ -rays reflects the activity of the central engine (as in the case of internal shocks⁹) this implies that t_{inj} determines the dominant crossover frequency. This frequency is below what can be achieved by any detector built on Earth. It is at the upper end of LISA's* bandwidth. However, the expected signal is about thousand times weaker than LISA's planned sensitivity (see Fig. 8). It falls nicely within the band of the proposed BBO and DEFIGO. However, a regular LGRB at a few Gpc is too far to be detected with the sensitivity reach of either BBO or DECIGO.

*<https://www.elisascience.org/>

6.1.2. Short GRBs and GRB 170817A

Short GRBs are associated with binary neutron star mergers,¹⁵ as demonstrated recently with the observations of GRB 170817A and the associated GW signal GW 170817.¹⁶ With typical energies of 10^{48-50} erg, sGRBs are much weaker than LGRBs. Correspondingly they are observed from nearer distances, typically of order 1 Gpc, with the nearest ones at distances of a few hundred Mpc (170817A was much nearer than average). Typical sGRB duration is less than 2 sec. The expected crossover frequency (which is again, presumable, is dominated by t_{inj} and not by t_{acc}) is of order 0.5-5 Hz. This is below current terrestrial detectors, it is too low even for the planned frequency band of more advanced detectors like the Einstein telescope[†]. Once more it falls within the planned frequency range of BBO and DECIGO. Again a typical sGRB at a few hundred Mpc is too far to be detected.

The exceptional sGRB, GRB 170817A, was sufficiently nearby that it could have been marginally detected with these advanced detectors. The properties of this well observed event are well known: $\mathcal{E} \approx 10^{50}$ erg, $\theta_v \approx 20^\circ$, $\theta_j \approx 5^\circ$.¹⁷ Other parameters, and in particular t_{acc} and t_{inj} that are most relevant for our analysis, are unknown. The injection duration t_{inj} , is not necessarily related to the duration of the observed γ -rays in this event, as those arose from a cocoon shock breakout.^{18,19} In the following we assume that $t_{\text{acc}} < t_{\text{inj}} \approx 1$ sec. Γ , is also unknown but it doesn't factor into the result as we expect $\Gamma^{-1} < \theta_j$ 0.1 rad. Given the viewing angle and the jet angle, GRB 170817A was also ideally positioned in terms of the strength of the GW signal from its jet. That is, we were not within the anti-beamed jet's cone but not too far from it either. The jet-GW of GRB 170717A signal was not detected. This is not surprising. Fig. 8, depicts the spectral density of GRB170817A compared with the sensitivity thresholds of GW detectors.⁸ It is below the frequency band of both LIGO and Virgo and also well below their sensitivity. Jet-GW from 170817 would have been detectable by BBO or DECIGO had such detector been operational at the time!

6.2. Hidden jets in Core-Collapse Supernovae (CCSNe) and low-luminosity GRBs (*llGRBs*)

Shortly after the discovery of the first *llGRB* 980415 (that was associated with SN98bw) it was suggested²⁰⁻²² that the emission arose from shock breakout following an energetic jet that was choked deep in the accompanying star. Later on it was realized that, while the detection rate of *llGRBs* is much lower than that of regular long ones, their actual rate is orders of magnitude larger.^{23,24} The detection rate is low because, given their low luminosity, they are detected only from relatively short distances. More recently, it was shown²⁵ that a significant fraction of CCSNe that are not necessarily associated with GRBs contain energetic ($\sim 10^{51}$ erg) choked relativistic jets. Such a jet deposits all its energy into a cocoon. Upon breakout

[†]<http://www.et-gw.eu/>

the cocoon material is observed as a high velocity (0.1-0.2c) material that engulfs the supernova and can be observed within the first few days. Such signatures have been detected²⁶ as early as 1997 in SN 1997EF and in several other SNe since then. This suggestion was nicely confirmed with the exquisite observations of this high velocity material in SN 2017iuk.^{27,28} It is supported by other evidence for jets in SNe.²⁹⁻³³

If such relativistic jets are associated with a significant fraction of CCSNe then, as the supernova rate is significantly larger than the GRB rate,³⁴ we can expect a significant number of relatively nearby jets that would be sources of jet-GWs. Comparing relativistic CCSNe Jets with GRB jets, we estimate a typical CCSN h to be a factor of 10 larger than the one from a typical long GRB. As we don't have a good clue on t_{inj} we assume that it is of the same order as the one estimated in long GRB, namely a few tens of seconds. Thus, the crossover frequency would be around 0.01 Hz.

If the event is accompanied by a l GRB (arising from the shock breakout of the cocoon) then there will be almost simultaneous EM signal associated with the GW signal (typical delays could be of order of a dozen seconds). However, if the event is not associated with a l GRB then the EM counterpart in the form of a supernova will emerge a few hours or even days after the GW signal.

6.3. Giant SGR Flares

Magnetars with magnetic fields larger than 10^{15} Gauss are among the most surprising objects discovered.³⁵ Magnetars eject giant flares while rearranging their whole magnetic field.³⁶ Such flares have been observed roughly once per ten years within the Milky Way. The last one, from SGR1806-20 was observed in 2004.³⁷⁻⁴⁰ It involved the acceleration of $\approx 10^{47}$ erg within a few milliseconds. The corresponding frequency is within the range of current GW detectors. With a Galactic distance the signal might be detectable if the initial injection was beamed. If these flares involve a jet of such energy then they could be detected even with current GW detectors up to distances of a few kpc. Proposed more advanced detectors could observe them from the whole Galaxy or even from M31.

6.4. Contribution to the GW background

The relativistic jets that arise from GRBs (both long and short) and hidden jets in SNe produce a background of jet-GW waves at frequency range of $\sim 0.01 - 1$ Hz depending on the specific source. Both long and short GRBs are rare and won't make a significant contribution to such a background. However, CCSNe take place at a rate of about one per second in the observable Universe. If a significant fraction of SNe harbor energetic jets the time between two such cosmological events, a few seconds, will be comparable to the characteristic time scale of the GW signals from these jets (assuming that the hidden jets in CCSNe are similar in nature to GRB

jets). Depending on the ratio of the time between events and the characteristic frequency of the jet-GW signal we expect either a continuous background, as expected from the GW background from merging binary neutron stars, or a pop-corn like signature, as expected for the GW background from merging binary black holes.⁴¹ With a typical cosmological distance of a few Gpc the corresponding amplitude of this jet-GW background is $h \approx 10^{-26} \mathcal{E}/(10^{51} \text{erg})$. With energy input of about 10^{41} erg in GW per SNe (see Eq. 6) and SN rate of about one per second in the Universe the resulting energy density of GW of this kind in the 0.1 Hz would be $\Omega_{\text{jet-GW}} \approx 10^{-9}$. Note, however, that there is an uncertainty of at least an order of magnitude due to the unclear t_c of this signal.

7. Discussion

The acceleration of a jet to a relativistic velocity generates a unique memory type GW signal. The signal is anti-beamed away from the direction of the jet with an anti-beaming angle of $\max(\Gamma^{-1}, \theta_j)$. Like typical relativistic GW sources, the amplitude is of order $G\mathcal{E}/c^4 r$, corresponding to an amplitude of $h \approx 10^{-24}$ for a jet of 10^{51} erg at 100 Mpc. At low frequencies the signal can be approximated as a step function. This last feature is of course problematic, as it might be difficult to distinguish it from step function type noise sources. At higher frequencies the details of the signal lightcurve could reveal information about the acceleration and collimation of the jet.

Prospects for detection of these jet-GWs depend on construction of appropriate future detectors. Jets from different kinds of GRBs as well as hidden jets in CCSNe are expected in the deciHz range. Hence most important are detectors like the proposed BBO, DECIGO and several moon detectors (e.g. LWGA, LSGA). Among those sources hidden jets in CCSNe are the best candidates as they are most frequent and as their expected energy is comparable to those of LGRBs.

As jet-GWs are anti-beamed we will most likely miss the γ -rays associated with GRBs from which we will observe these GWs. However, we expect to observe other associated wider signatures such as the afterglow or an accompanying shock breakout signal from the stellar envelope (in case of a LGRB) or from the merger's ejecta (in a sGRB). This shock breakout signal is also the most likely EM signal associated temporarily with a jet-GW arising from hidden jet in CCSN. In this case the actual SN signal may appear hours later.

Table 1 summarizes (under somewhat optimistic assumptions) the detection horizon of different events. Given the large uncertainties I didn't attempt to incorporate possible estimates of detection rates as these will be highly uncertain. Detection prospects with current detectors, LIGO, Virgo and Kagra that are operating at frequencies above 10 Hz are slim, unless giant SGR flare involve jets. In that case we could detect a Galactic event even with LVK. Otherwise we will have to resort to future planned detectors. What is most important is to remember that

these signals are memory type. Usually we are not looking for such astrophysical signals. We should make sure to expand GW searches to include such signatures in all future runs. A detection of Jet-GWs would open a new window on jet engines and would reveal features of jet acceleration in the vicinity of black holes that are impossible to explore in any other way.

Acknowledgments

The research was supported by an advanced ERC grant TReX.

References

1. B. P. Abbott et al. and LIGO Scientific Collaboration, Observation of Gravitational Waves from a Binary Black Hole Merger, *Phys. Rev. Lett.* . 116(6):061102 (Feb, 2016). doi: 10.1103/PhysRevLett.116.061102.
2. B. P. Abbott, et al., LIGO Scientific Collaboration, and Virgo Collaboration, GW170817: Observation of Gravitational Waves from a Binary Neutron Star Inspiral, *Phys. Rev. Lett.* . 119(16):161101 (Oct., 2017). doi: 10.1103/PhysRevLett.119.161101.
3. E. B. Segalis and A. Ori, Emission of gravitational radiation from ultrarelativistic sources, *Phys. Rev. D.* . 64(6):064018 (Sep, 2001). doi: 10.1103/PhysRevD.64.064018.
4. T. Piran. Gamma-Ray Bursts - a Primer for Relativists. In eds. N. T. Bishop and S. D. Maharaj, *General Relativity and Gravitation*, pp. 259–275 (Sept., 2002). doi: 10.1142/9789812776556_0013.
5. N. Sago, K. Ioka, T. Nakamura, and R. Yamazaki, Gravitational wave memory of gamma-ray burst jets, *Phys. Rev. D.* **70**, 104012, (2004). doi: 10.1103/PhysRevD.70.104012.
6. O. Birnholtz and T. Piran, Gravitational wave memory from gamma ray bursts' jets, *Phys. Rev. D.* . 87(12):123007 (Jun, 2013). doi: 10.1103/PhysRevD.87.123007.
7. E. Leiderschneider and T. Piran, Gravitational radiation from accelerating jets, *Phys. Rev. D.* . 104(10):104002 (Nov., 2021). doi: 10.1103/PhysRevD.104.104002.
8. C. J. Moore, R. H. Cole, and C. P. L. Berry, Gravitational-wave sensitivity curves, *Classical and Quantum Gravity*. **32**(1), 015014 (Dec, 2014). ISSN 1361-6382. doi: 10.1088/0264-9381/32/1/015014. URL <http://dx.doi.org/10.1088/0264-9381/32/1/015014>.
9. S. Kobayashi, T. Piran, and R. Sari, Can Internal Shocks Produce the Variability in Gamma-Ray Bursts?, *ApJ*. **490**, 92 (Nov., 1997). doi: 10.1086/512791.
10. J. Harms, F. Ambrosino, L. Angelini, V. Braitto, M. Branchesi, E. Brocato, E. Cappellaro, E. Coccia, M. Coughlin, R. Della Ceca, M. Della Valle, C. Dionisio, C. Federico, M. Formisano, A. Frigeri, A. Grado, L. Izzo, A. Marcelli, A. Maselli, M. Olivieri, C. Pernechele, A. Possenti, S. Ronchini, R. Serafinelli, P. Severgnini, M. Agostini, F. Badaracco, A. Bertolini, L. Betti, M. M. Civitani, C. Collette, S. Covino, S. Dall'Osso, P. D'Avanzo, R. DeSalvo, M. Di Giovanni, M. Focardi, C. Giunchi, J. van Heijningen, N. Khetan, D. Melini, G. Mitri, C. Mow-Lowry, L. Naponiello, V. Noce, G. Oganessian, E. Pace, H. J. Paik, A. Pajewski, E. Palazzi, M. Pallavicini, G. Pareschi, R. Pozzobon, A. Sharma, G. Spada, R. Stanga, G. Tagliaferri, and R. Votta, Lunar Gravitational-wave Antenna, *ApJ*. 910(1):1 (Mar., 2021). doi: 10.3847/1538-4357/abe5a7.
11. S. Katsanevas, P. Bernard, D. Giardini, P. Jousset, P. Mazzali, P. Lognonné, E. Pian, A. Amy, T. Apostolatos, M. Barsuglia, et al., in *Ideas for exploring the Moon with a large European lander* (ESA, 2020), p. 1, URL <https://ideas.esa.int/servlet/hype/IMT?documentTableId=45087607031744010&userAction=Browse&templateName=&documentId=a315450fae481074411ef65e4c5b7746>
12. J. Crowder and N. J. Cornish, Beyond LISA: Exploring future gravitational wave missions, *Phys. Rev. D.* . 72(8):083005 (Oct., 2005). doi: 10.1103/PhysRevD.72.083005. @ARTICLEMoore2015, author = Moore, C. J. and Cole, R. H. and Berry, C. P. L., title = "Gravitational-wave sensitivity curves", journal = Classical and Quantum Gravity, keywords = gravitational waves, black holes, pulsar timing, pulsar timing arrays, 04.30.-w, 04.30.Db, 04.80.Nn, 95.55.Ym, General Relativity and Quantum Cosmology, Astrophysics - High Energy Astrophysical Phenomena, year = 2015, month =

Acknowledgments

17

- jan, volume = 32, number = 1, eid = 015014, pages = 015014, doi = 10.1088/0264-9381/32/1/015014, archivePrefix = arXiv, eprint = 1408.0740, primaryClass = gr-qc, adsurl = <https://ui.adsabs.harvard.edu/abs/2015CQGra..32a5014M>, adsnote = Provided by the SAO/NASA Astrophysics Data System
13. S. Sato et al. The status of DECIGO. In *Journal of Physics Conference Series*, vol. 840, p. 012010 (May, 2017). doi: 10.1088/1742-6596/840/1/012010.
 14. A. M. Beloborodov, Power density spectra of gamma-ray bursts, *AIP Conference Proceedings*. (2000). ISSN 0094-243X. doi: 10.1063/1.1361535. URL <http://dx.doi.org/10.1063/1.1361535>.
 15. D. Eichler, M. Livio, T. Piran, and D. N. Schramm, Nucleosynthesis, neutrino bursts and gamma-rays from coalescing neutron stars, *Nature*. **340**, 126–128 (July, 1989). doi: 10.1038/340126a0.
 16. B. P. Abbott, et al., LIGO Scientific Collaboration, and Virgo Collaboration, Multimessenger Observations of a Binary Neutron Star Merger, *ApJL*. 848(2):L12 (Oct, 2017). doi: 10.3847/2041-8213/aa91c9.
 17. E. Nakar, The electromagnetic counterparts of compact binary mergers, *Phys. Reports*. **886**, 1–84 (Nov., 2020). doi: 10.1016/j.physrep.2020.08.008.
 18. M. M. Kasliwal, E. Nakar, L. P. Singer, D. L. Kaplan, D. O. Cook, A. Van Sistine, R. M. Lau, C. Fremling, O. Gottlieb, J. E. Jencson, S. M. Adams, U. Feindt, K. Hotokezaka, S. Ghosh, D. A. Perley, P. C. Yu, T. Piran, J. R. Allison, G. C. Anupama, A. Balasubramanian, K. W. Bannister, J. Bally, J. Barnes, S. Barway, E. Bellm, V. Bhalariao, D. Bhattacharya, N. Blagorodnova, J. S. Bloom, P. R. Brady, C. Cannella, D. Chatterjee, S. B. Cenko, B. E. Cobb, C. Copperwheat, A. Corsi, K. De, D. Dobie, S. W. K. Emery, P. A. Evans, O. D. Fox, D. A. Frail, C. Frohmaier, A. Goobar, G. Hallinan, F. Harrison, G. Helou, T. Hinderer, A. Y. Q. Ho, A. Horesh, W. H. Ip, R. Itoh, D. Kasen, H. Kim, N. P. M. Kuin, T. Kupfer, C. Lynch, K. Madson, P. A. Mazzali, A. A. Miller, K. Mooley, T. Murphy, C. C. Ngeow, D. Nichols, S. Nissanke, P. Nugent, E. O. Ofek, H. Qi, R. M. Quimby, S. Rosswog, F. Rusu, E. M. Sadler, P. Schmidt, J. Sollerman, I. Steele, A. R. Williamson, Y. Xu, L. Yan, Y. Yatsu, C. Zhang, and W. Zhao, Illuminating gravitational waves: A concordant picture of photons from a neutron star merger, *Science*. **358**(6370), 1559–1565 (Dec., 2017). doi: 10.1126/science.aap9455.
 19. O. Gottlieb, E. Nakar, T. Piran, and K. Hotokezaka, A cocoon shock breakout as the origin of the γ -ray emission in GW170817, *MNRAS*. **479**(1), 588–600 (Sept., 2018). doi: 10.1093/mnras/sty1462.
 20. S. R. Kulkarni, D. A. Frail, M. H. Wieringa, R. D. Ekers, E. M. Sadler, R. M. Wark, J. L. Higdon, E. S. Phinney, and J. S. Bloom, Radio emission from the unusual supernova 1998bw and its association with the γ -ray burst of 25 April 1998, *Nature*. **395**(6703), 663–669 (Oct., 1998). doi: 10.1038/27139.
 21. A. I. MacFadyen, S. E. Woosley, and A. Heger, Supernovae, Jets, and Collapsars, *ApJ*. **550**(1), 410–425 (Mar., 2001). doi: 10.1086/319698.
 22. J. C. Tan, C. D. Matzner, and C. F. McKee, Trans-Relativistic Blast Waves in Supernovae as Gamma-Ray Burst Progenitors, *ApJ*. **551**(2), 946–972 (Apr., 2001). doi: 10.1086/320245.
 23. A. M. Soderberg, S. R. Kulkarni, E. Nakar, E. Berger, P. B. Cameron, D. B. Fox, D. Frail, A. Gal-Yam, R. Sari, S. B. Cenko, M. Kasliwal, R. A. Chevalier, T. Piran, P. A. Price, B. P. Schmidt, G. Pooley, D. S. Moon, B. E. Penprase, E. Ofek, A. Rau, N. Gehrels, J. A. Nousek, D. N. Burrows, S. E. Persson, and P. J. McCarthy, Relativistic ejecta from X-ray flash XRF 060218 and the rate of cosmic explosions, *Nature*. **442**(7106), 1014–1017 (Aug., 2006). doi: 10.1038/nature05087.

24. O. Bromberg, E. Nakar, and T. Piran, Are Low-luminosity Gamma-Ray Bursts Generated by Relativistic Jets?, *ApJL*. 739(2):L55 (Oct, 2011). doi: 10.1088/2041-8205/739/2/L55.
25. T. Piran, E. Nakar, P. Mazzali, and E. Pian, Relativistic Jets in Core Collapse Supernovae, *Astrophys. J.* **871**(2), L25, (2019). doi: 10.3847/2041-8213/aaffce.
26. P. A. Mazzali, K. Iwamoto, and K. Nomoto, A Spectroscopic Analysis of the Energetic Type Ic Hypernova SN 1997EF, *ApJ*. **545**(1), 407–419 (Dec., 2000). doi: 10.1086/317808.
27. L. Izzo, A. de Ugarte Postigo, K. Maeda, C. C. Thöne, D. A. Kann, M. Della Valle, A. Sagues Carracedo, M. J. Michałowski, P. Schady, S. Schmidl, J. Selsing, R. L. C. Starling, A. Suzuki, K. Bensch, J. Bolmer, S. Campana, Z. Cano, S. Covino, J. P. U. Fynbo, D. H. Hartmann, K. E. Heintz, J. Hjorth, J. Japelj, K. Kamiński, L. Kaper, C. Kouveliotou, M. Krużyński, T. Kwiatkowski, G. Leloudas, A. J. Levan, D. B. Malesani, T. Michałowski, S. Piranomonte, G. Pugliese, A. Rossi, R. Sánchez-Ramírez, S. Schulze, D. Steeghs, N. R. Tanvir, K. Ulaczyk, S. D. Vergani, and K. Wiersema, Signatures of a jet cocoon in early spectra of a supernova associated with a γ -ray burst, *Nature*. **565**(7739), 324–327 (Jan., 2019). doi: 10.1038/s41586-018-0826-3.
28. E. Nakar, Heart of a stellar explosion revealed, *Nature*. **565**(7739), 300–301 (Jan., 2019). doi: 10.1038/d41586-019-00043-x.
29. T. Totani, A Failed Gamma-Ray Burst with Dirty Energetic Jets Spirited Away? New Implications for the Gamma-Ray Burst-Supernova Connection from SN 2002ap, *ApJ*. **598**, 1151–1162 (Dec., 2003). doi: 10.1086/378936.
30. P. A. Mazzali, K. S. Kawabata, K. Maeda, K. Nomoto, A. V. Filippenko, E. Ramirez-Ruiz, S. Benetti, E. Pian, J. Deng, N. Tominaga, Y. Ohyama, M. Iye, R. J. Foley, T. Matheson, L. Wang, and A. Gal-Yam, An Asymmetric Energetic Type Ic Supernova Viewed Off-Axis, and a Link to Gamma Ray Bursts, *Science*. **308**, 1284–1287 (May, 2005). doi: 10.1126/science.1111384.
31. K. Maeda, K. Kawabata, P. A. Mazzali, M. Tanaka, S. Valenti, K. Nomoto, T. Hattori, J. Deng, E. Pian, S. Taubenberger, M. Iye, T. Matheson, A. V. Filippenko, K. Aoki, G. Kosugi, Y. Ohyama, T. Sasaki, and T. Takata, Asphericity in Supernova Explosions from Late-Time Spectroscopy, *Science*. **319**, 1220 (Feb., 2008). doi: 10.1126/science.1149437.
32. S. Taubenberger, S. Valenti, S. Benetti, E. Cappellaro, M. Della Valle, N. Elias-Rosa, S. Hillebrandt, W. Hillebrandt, K. Maeda, P. A. Mazzali, A. Pastorello, F. Patat, S. A. Sim, and M. Turatto, Nebular emission-line profiles of Type Ib/c supernovae - probing the ejecta asphericity, *MNRAS*. **397**, 677–694 (Aug., 2009). doi: 10.1111/j.1365-2966.2009.15003.x.
33. A. Grichener and N. Soker, Core collapse supernova remnants with ears, *MNRAS*. **468**, 1226–1235 (June, 2017). doi: 10.1093/mnras/stx534.
34. T. Piran, Gamma-ray bursts and the fireball model, *Phys. Rept.* **314**, 575–667, (1999). doi: 10.1016/S0370-1573(98)00127-6.
35. C. Kouveliotou, T. Strohmayer, K. Hurley, J. van Paradijs, M. H. Finger, S. Dieters, P. Woods, C. Thompson, and R. C. Duncan, Discovery of a Magnetar Associated with the Soft Gamma Repeater SGR 1900+14, *ApJL*. **510**(2), L115–L118 (Jan., 1999). doi: 10.1086/311813.
36. D. Eichler, Waiting for the Big One: a new class of soft gamma-ray repeater outbursts?, *MNRAS*. **335**(4), 883–886 (Oct., 2002). doi: 10.1046/j.1365-8711.2002.05571.x.
37. K. Hurley, S. E. Boggs, D. M. Smith, R. C. Duncan, R. Lin, A. Zoglauer, S. Krucker, G. Hurford, H. Hudson, C. Wigger, W. Hajdas, C. Thompson, I. Mitrofanov, A. Sanin,

Acknowledgments

19

- W. Boynton, C. Fellows, A. von Kienlin, G. Lichti, A. Rau, and T. Cline, An exceptionally bright flare from SGR 1806-20 and the origins of short-duration γ -ray bursts, *Nature*. **434**(7037), 1098–1103 (Apr., 2005). doi: 10.1038/nature03519.
38. S. Mereghetti, D. Götz, A. von Kienlin, A. Rau, G. Lichti, G. Weidenspointner, and P. Jean, The First Giant Flare from SGR 1806-20: Observations Using the Anticoincidence Shield of the Spectrometer on INTEGRAL, *ApJL*. **624**(2), L105–L108 (May, 2005). doi: 10.1086/430669.
 39. D. M. Palmer, S. Barthelmy, N. Gehrels, R. M. Kippen, T. Cayton, C. Kouveliotou, D. Eichler, R. A. M. J. Wijers, P. M. Woods, J. Granot, Y. E. Lyubarsky, E. Ramirez-Ruiz, L. Barbier, M. Chester, J. Cummings, E. E. Fenimore, M. H. Finger, B. M. Gaensler, D. Hullinger, H. Krimm, C. B. Markwardt, J. A. Nousek, A. Parsons, S. Patel, T. Sakamoto, G. Sato, M. Suzuki, and J. Tueller, A giant γ -ray flare from the magnetar SGR 1806 - 20, *Nature*. **434**(7037), 1107–1109 (Apr., 2005). doi: 10.1038/nature03525.
 40. T. Terasawa, Y. T. Tanaka, Y. Takei, N. Kawai, A. Yoshida, K. Nomoto, I. Yoshikawa, Y. Saito, Y. Kasaba, T. Takashima, T. Mukai, H. Noda, T. Murakami, K. Watanabe, Y. Muraki, T. Yokoyama, and M. Hoshino, Repeated injections of energy in the first 600ms of the giant flare of SGR1806 - 20, *Nature*. **434**(7037), 1110–1111 (Apr., 2005). doi: 10.1038/nature03573.
 41. B. P. e. a. Abbott, LIGO Scientific Collaboration, and Virgo Collaboration, GW170817: Implications for the Stochastic Gravitational-Wave Background from Compact Binary Coalescences, *Phys. Rev. Lett.* . 120(9):091101 (Mar., 2018). doi: 10.1103/PhysRevLett.120.091101.